# VALIDATION OF THE AKR-2 REACTOR SIMPLIFIED MODEL USING OPENMC AND SERPENT: A DEEP ANALYSIS OF THE PILE OSCILLATOR EXPERIMENT

J.J. GÓMEZ RODRIGUEZ, C. LANGE, M. VIEBACH, A. KNOSPE, A. HURTADO
*Chair of Hydrogen and Nuclear Energy, Technische Universität Dresden*
*Helmholtzstraße 9, 01069, Dresden - Germany*

V. GIUSTI
*Department of Civil and Industrial Engineering, University of Pisa*
*Largo L. Lazzarino, 56126, Pisa - Italy*

## ABSTRACT

The AKR-2 reactor at TU Dresden is a solid-moderated, thermal zero-power reactor used for training and research. This study validates the simplified AKR-2 model using Monte Carlo codes OpenMC and Serpent, comparing simulations with experimental data. Measurements include neutron flux in experimental channels, reactivity curves of shutdown devices, and pile oscillator experiments. The pile oscillator experiment involves periodic sample motion in an axial channel, testing samples made of iridium, indium, gold, hafnium, copper, zirconium, and graphite. By analysing amplitude signals, macroscopic absorption cross-section ratios between material pairs were determined. Experimental and simulated results showed deviations of 10-20%. Additionally, $k_{eff}$ criticality simulations replicated computationally the experimental reactivity oscillations. The range of frequencies, motion profiles, and materials provided lessons learned in the pile oscillator experiment and provided a way to obtain integral data of multiple materials at this facility. The validation marks progress toward detailed AKR-2 models currently under development.

## 1. Introduction

The zero-power nuclear reactor AKR-2 located at TU Dresden is used for research and training. It provides students, operators, and researchers with the possibility to assimilate knowledge in reactor operation and physics. A series of experiments, designed for this reactor, include the critical experiment, control rod calibration, adjoint flux function, radial flux distribution, pile oscillator experiment, activation, and others [1][2]. The simulation of these experiments with Monte Carlo codes in a full and detailed model of the reactor, as done in the context of the NAUTILUS project [3], implies a large computational effort, variance reduction techniques, and running time which may pose a difficulty in a teaching and research environment. Then, Serpent [4] and OpenMC [5] simplified models were developed. This study seeks to probe the suitability of these models to provide reliable and comparable results to those obtained experimentally at the AKR-2, focusing on the pile oscillator and its validation.

## 2. The AKR-2 simplified model

The AKR-2 simplified model (see Fig. 1) consists of the core made of a homogeneous mixture of low enriched uranium (19.8%) and solid polyethylene which serves as moderator. The core is a cylinder of 12.5 cm radius and around 28 cm height which is divided into two sections, the lower and upper core half. When the reactor is made critical, both sections are joined, and shutdown is achieved by letting the lower core half drop by gravity. The core is surrounded by an inner and outer reflector made of graphite. The outer reflector contains three air gaps where the control rods are located. The control rods are made of polyethylene blocks with cadmium sheets attached to them. There are four experimental channels. Channel 1-2 is a horizontal channel going through the centre of the core, channels 3-4 and 5-6 are tangential channels

going through the reflector, and channel 7, leads from the surface of the reactor to the reactor core. It includes a vertical channel for the start-up neutron source (see Fig. 1).

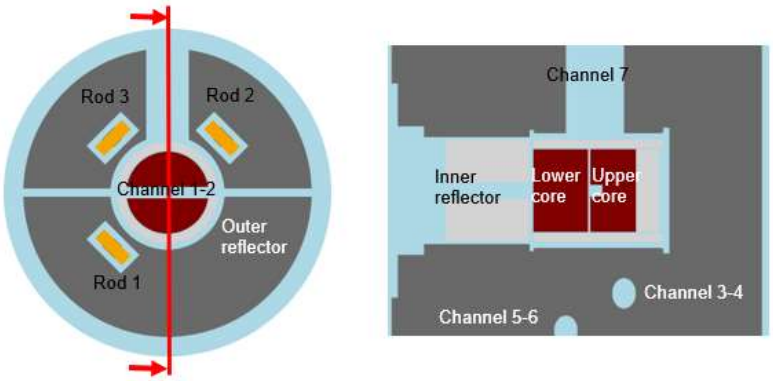


Figure 1: Top (left) and lateral (right) view of the reactor geometry.

The simple model differs from the actual reactor geometry in multiple geometry simplifications, the channel 7 shape, the paraffin surrounding the outer reflector, the biological shielding made of concrete and structures such as joints and coatings made of aluminium alloys and iron.

## 3. Reactor experiments

Details of the experiments performed at the reactor can be found in [1]. Here, a few experimental details are given, but the attention will be laid on the results obtained experimentally, and the validation of the simplified AKR-2 model in OpenMC and Serpent. To verify that the two models are consistent to each other, material and geometry definitions were checked. To do so, the occupied volume was computed for every material and cell in the reactor as can be seen in table 1.

| Material | OpenMC ($cm^3$) | Serpent ($cm^3$) |
|---|---|---|
| Fuel/Moderator mix | 13293.5 ± 4.8 | 13285.2 ± 3.1 |
| Inner reflector | 27044.5 ± 1.7 | 27041.3 ± 0.9 |
| Polyethylene | 5564.4 ± 0.3 | 5563.9 ± 0.7 |
| Cadmium | 54.12 ± 0.31 | 54.10 ± 0.61 |
| Outer reflector | 507565.1 ± 2.5 | 507571.0 ± 3.3 |
| Air | 848636 ± 28 | 848625 ± 40 |

Table 1: Simulated material volumes

Volume calculations provided assurance about cells sizes. Also, multiple slice plots were generated and overlapped. Careful attention was given to the use of the cross sections' library. In Serpent, we used ENDF/B-VIII.0 [6], and to assure that OpenMC used the same, cross sections datafiles needed in OpenMC were generated from the used in Serpent.

### 3.1 Critical Experiment

The critical experiment is performed to check that the reactor may become critical with the current core load. The lower core half is approached to the fixed upper core half, this is done stepwise by moving the lower core half up to five centimetres. The multiplication factor of the reactor $k_{\mathrm{eff}}$ will depend on the distance $z_{\mathrm{i}}$ between the lower and upper core half (the subindex i indicates the step the lower core half is moved). When the lower core half is at the lowest position, the multiplication factor corresponds to $k_0 = k(z_0)$. This value is assumed to be given by the average value between Serpent and OpenMC. It can be shown that the multiplication factor at the next step [1], i.e., at a higher lower core half position is given by:

$$k(z_i + \Delta z) = 1 + \frac{N(z_i)}{N(z_i + \Delta z)} (k(z_i) - 1) \quad (1)$$

The counting rates $N(z_i)$ and $N(z_i + \Delta z)$ were measured by a fission chamber and a $BF_3$ detector in the outer reflector region. Experimentally, the multiplication factor at the next step can be obtained iteratively. The $k_0$ used for this experiment was (0.93125 +/- 0.00005). The reactivity insertion, $\rho(z_i)$, when approaching the upper core half is:

$$\rho(z_i) = \frac{k(z_i) - 1}{k(z_i)} \quad (2)$$

The main MC criticality simulation parameters were 80 inactive batches, 120 active batches and 2,000,000 particles per batch for all the simulations here presented, unless stated otherwise. Uncertainties are always reported as two times the standard deviation, $2\sigma$.

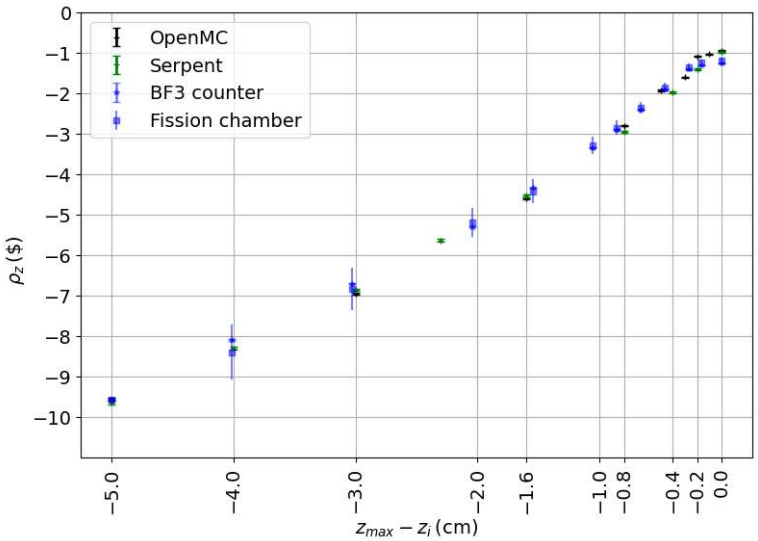


Figure 2: Reactivity insertion due to lower core half approach.

When the lower core half reaches its uppermost position, the reactivity is around -1$ because the three control rods are inserted. This experiment can also be performed with the control rods out, taking care that when the lower core half approaches its end position, the reactor becomes supercritical. Good agreement between experimental and simulated values is visible over all the positions of the lower core half. The plateau observed experimentally from -0.2 cm to 0 cm (see Fig.2) occurs because the lower core half touches the upper core half and pushes it upwards. The MC models treat this by moving upwards both lower and upper core halves a few millimetres.

### 3.2 Control Rod Calibration

The control rod calibration aims to obtain the integral and differential rod worth curves; this is done by using the stable period $T_s$ of the reactor when an insertion of positive reactivity is done by a rod. An acrylic cylinder is inserted inside of the channel 1-2 during the experiment to increase the reactivity of the reactor due to its moderator effect. In this way, the reactor may reach the critical state with one control rod fully inserted. The rods in the AKR-2 can be moved between 0 and 4000 digits. They are considered fully inserted when the visualization panel displays the position 0 and fully withdrawn when it is 4000, which corresponds to a movement of the rod by 38.5 cm. The reactivity insertion $\rho'$ in dollars (1$ = 100 ct) can be written as:

$$\rho' = \frac{\rho}{\beta} = \frac{l'}{\beta T_s} + \sum_{i=1}^{6} \frac{\beta_i/\beta}{1 + \lambda_i T_s} \quad (3)$$

The fraction of delayed neutrons $\beta$ used for these calculations is (7.6715 ± 0.0099) x $10^{-3}$. The average effective lifetime of prompt neutrons $l'$ is (5.6688 ± 0.0020) x $10^{-5}$ s. Six groups of precursors are used, $\lambda_i$ and $\beta_i$ represent the group decay constants and their fraction of delayed neutrons. The measurement implies to make the reactor critical at some power by having one fully inserted and one fully withdrawn control rod. Then, the stable reactor period method is used. As a result, the reactivity curves of the two control rods are determined. If the reactivity curves of all control rods are known, the excess reactivity and shutdown reactivity can be calculated. Moreover, the reactivity curve of an arbitrary sample can be determined in terms of a change of the critical control rod position.

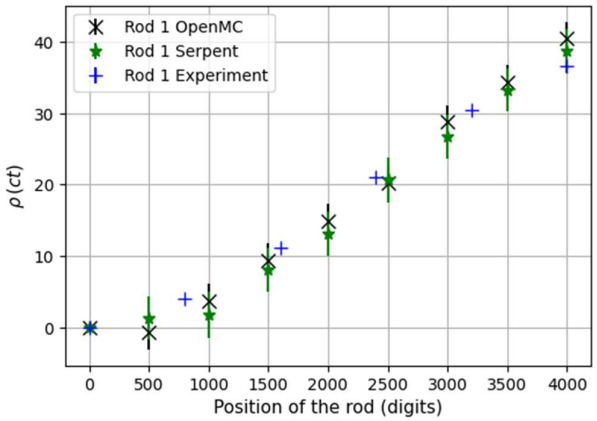


Figure 3: Integral worth curve for rod one.

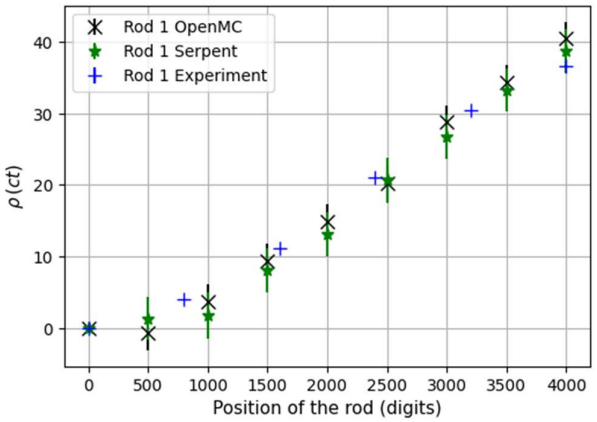


Figure 4: Integral worth curve for rod two.

Unfortunately, the exact position reached by the rods when they are fully inserted is unknown. A parametric study on the full insertion position was done for each rod. Thus, comparing the obtained worth curves with the experimental ones it was possible to estimate the correct full insertion position of each one of them. Moreover an air gap of 14 cm was added at the top of each rod to allocate the pulleys (although, not included in the MC models) that move them up and down. Then, the top of the control rods in shutdown position is (7 ± 1) cm higher than the top of the upper core half. Moreover, the space for the structural materials which drive the rods (above the rods) must be (14 ± 1) cm.

As shown by Fig. 3, 4, and 5, the Serpent and OpenMC results are similar to those obtained experimentally, thus confirming the quality of the models and their consistency with each other.

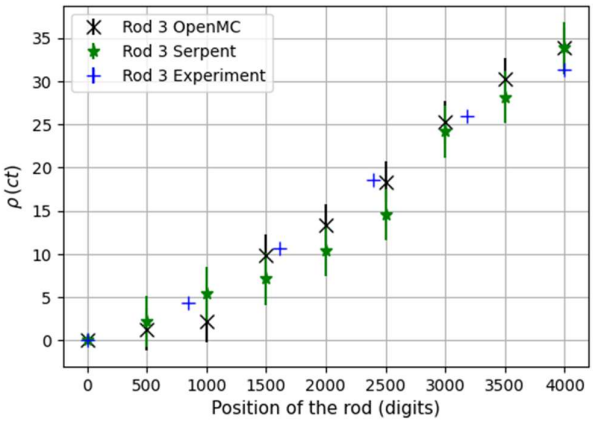


Figure 5: Integral worth curve for rod three.

### 3.3 Radial Flux Measurement

Thirty-one samples of manganese-copper alloy in a probe were activated inside channel 1-2 of the AKR-2. Manganese has only one stable isotope, and when it captures a neutron, it undergoes beta decay accompanied by characteristic gamma rays, producing Iron-56 with a half-life of 2.58 h. The activity of these samples after irradiation is an indirect indication of the radial flux. The activity of the samples was measured with a NaI(Tl)-scintillation detector. A negligible self-shielding is assumed as the cylindrical foils have a thickness around 40 μm and a radius of 1.4 cm.

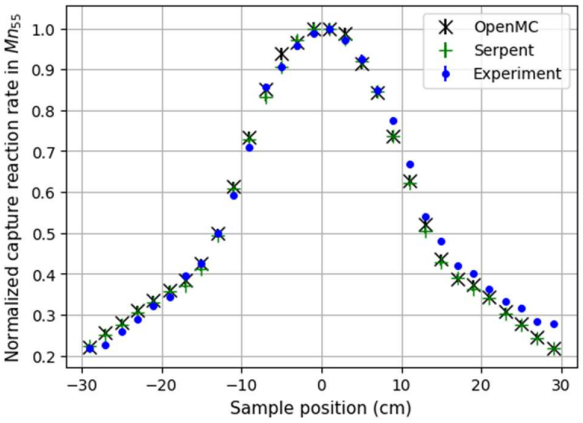


Figure 6: Capture reaction rate in channel 1-2.

The Serpent simulations scored the capture reaction rate inside a cylindrical mesh, 2 cm thick, along the channel 1-2. In OpenMC, the capture reaction rate is scored within samples of manganese placed in correspondence of the midpoint of the Serpent mesh elements. The small asymmetry in the radial flux distribution shown by the simulation and experimental results is due to the asymmetric configuration of the air channels for the control rods (see Fig. 1). As a matter of fact, a larger portion of reflector is present on the right side of the channel 1-2. However, both simulations produce a more symmetric distribution at the edge of the measured range. Probably, the large neutron leakages, due to the lack of the paraffine and concrete in the simplified models, makes the above effect less relevant.

### 3.4 Reactivity Worth Curves

Changes in the multiplication factor, $k_{\text{eff}}$, of the reactor due to the introduction of a sample into it depend on the sample material and where it is located. For absorbing samples, the inserted

reactivity is proportional to the product of the integral averaged macroscopic absorption cross section $\Sigma_a$(averaged with the spectrum of the reactor) and the second power of the neutron flux $\varphi^2(\vec{r})$ at the sample position. Instead, for materials with a large integral averaged scattering cross section with respect to absorption, $\Sigma_s \gg \Sigma_a$ , the inserted reactivity is proportional to the second power of the gradient of the flux $(\nabla\varphi)^2$. From now on, the latter materials will be referred to as scatterers. In this experiment, thin circular foils of different materials are inserted in a cylindrical container made of an aluminium alloy. The container is then placed in a bar driven by a linear motor axis inside channel 1-2 (see Fig. 7). The position of the container within the rod may be modified by an adequate arrangement of paperboard cylinders in the bar.

Figure 7: Linear motor and bar inserted in channel 1-2.

The samples are moved every 2 cm between the centre and 20 cm to the left of the core in channel 1-2. Initially, the sample is in the centre, rods two and three are extracted and rod one is used to achieve criticality. The rod compensation method using the integral worth curve of rod one (see Fig. 3) is then used to determine the relative reactivity $\rho_r(x)$ inserted when the sample is in the position $x$ respect to the reactivity when it is at the centre ($x$=0):

$$\rho_{\mathrm{r}}\,(x) = \rho_1(0) - \rho_1\,(x) \tag{4}$$

Samples of hafnium, indium, and iridium, with thicknesses ranging between 100 and 150 μm were used. To reduce the uncertainties on the changes of $k_{\mathrm{eff}}$ induced by a 2 cm movement of these small samples, for this experiment the number of particles per batch in the MC simulations was increased from 2 to 80 million. The reactivity measurements were obtained subtracting from the values given by each sample the contribution due to the empty container (that was measured separately).

The uncertainties associated with the measured reactivity values (see Fig. 8) are due to oscillations in the position of the control rod one due to the controller. The non-negligible power drift of the reactor was managed through 1) cooling for several days the reactor building to achieve stable temperatures, thus reducing temperature-related effects; 2) performing the measurements in forward and reverse increments (i.e. from 0 cm to 20 cm and back) thus ensuring thorough data collection across the displacement range.

Deviations between simulated and experimental values are outside estimated uncertainties for the iridium, while more consistent for hafnium and indium. The insertion of reactivity due to the iridium foil ranges between 0 and 5 ct, while from 0 to 2 ct for indium, and hafnium. Simulations were also performed for gold and copper thin foils. The gold foil did not output significant changes in $k_{\mathrm{eff}}$, due to its small thickness, 30 μm. The same happened with the copper foil, despite a thickness of 500 μm, due to the low absorption and scattering integral cross sections. Therefore, they are not shown in the Fig. 8. When these samples are moved with a periodic motion in the channel 1-2, this leads to oscillations of the reactor power. This is the experimental principle of the pile oscillator, where the reactivity curves obtained by the MC codes are used.

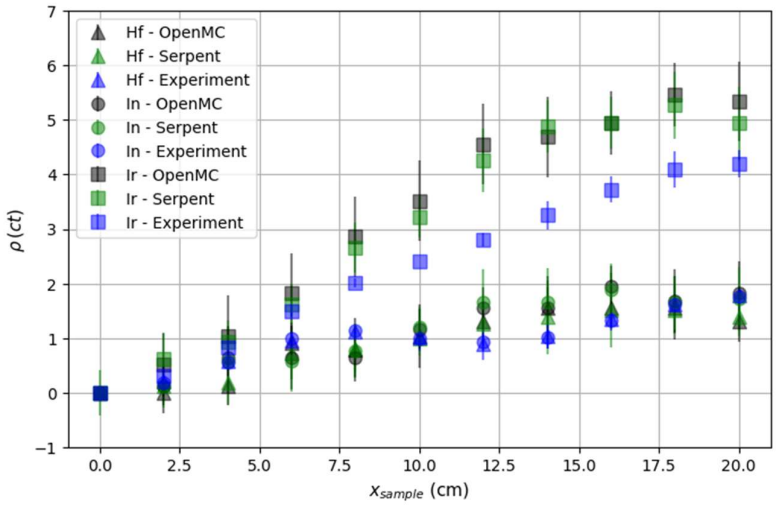


Figure 8: Reactivity insertion by placing samples at given positions in channel 1-2

## 4. Pile Oscillator

The pile oscillator method aims to obtain the integral absorption cross section of sample materials [6]. The samples are oscillated between different positions in the channel 1-2 using two motion profiles $x_{\text{sample}}(t)$: namely, a periodic step motion and a periodic constant speed motion (in the following also referred to as linear ramp). A periodic motion of low frequency, where the transfer function $H(i\omega)$ has a large amplitude, leads to large power oscillations, according to the following equation

$$\delta \mathrm{P}(\omega) = P_0 H(i\omega)\delta\rho(\omega) \tag{5}.$$

The experiment has been performed with the reactor critical around a power $P_0$ = 1.5 W. Two different frequencies were employed: $f_1 = \omega_1/2\pi = 0.005$ Hz and $f_2 = \omega_2/2\pi \approx 0.047$ Hz. If the sample is oscillated between positions where reactivity worth is maximum and minimum (see Fig. 8), the amplitude of the power oscillation in time and frequency domain is an indication of the integral absorption cross section.

Then, if two samples, A and B, are oscillated with the same profile and the same frequency, neglecting the self-shielding of the samples, the ratio of their power oscillations in the frequency domain is [1]:

$$\frac{P_{\mathrm{A}}(\omega)}{P_{\mathrm{B}}(\omega)} = \frac{\Sigma_{\mathrm{a,A}} m_{\mathrm{A}}/d_{\mathrm{A}}}{\Sigma_{\mathrm{a,B}} m_{\mathrm{B}}/d_{\mathrm{B}}} \tag{6}$$

The masses $m_{\mathrm{A}}, m_{\mathrm{B}}$, and the densities $d_A, d_B$ correct the fact that not all samples have the same volume. Samples of copper, gold, graphite, hafnium, indium, iridium, and zirconium, with thickness ranging from 30 to 500 μm, were used to achieve three objectives: *i*) validate the simulations for the pile oscillator; *ii*) validate the neutron energy spectrum obtained with Serpent and OpenMC in the channel 1-2; *iii*) obtain ratios between integral absorption cross sections, as shown by Eq. 6. These three objectives, however, had the main impediment of requiring large running time and computational effort to accurately estimate $k_{\text{eff}}$ obtain changes due to the displacement of a thin sample along the channel, particularly in the case of low absorbing materials. The convolution of the reactivity worth of the sample, $\rho(x)$, with the motion profile, $x_{\text{sample}}(t)$, allows writing the time dependent reactivity,

$$\rho(t) = \rho_{\mathrm{r}}\left(x_{\text{sample}}(t)\right). \tag{7}$$

Thus, comparing the experimental power oscillations $P(\omega)$ with the simulated reactivity time series in the frequency domain, $\rho(\omega)$, makes it possible to validate the simulations. The power ratios and the reactivity ratios between any two samples A and B are collected in the matrices $\mathbf{P_{AB}}(\omega)$ and $\boldsymbol{\rho_{AB}}(\omega)$, respectively its elements are:

$$\mathrm{P}_{AB}(\omega) = \frac{P_{\mathrm{A}}(\omega)}{P_{\mathrm{B}}(\omega)} \; ; \; \rho_{AB}(\omega) = \frac{\rho_{\mathrm{A}}(\omega)}{\rho_{\mathrm{B}}(\omega)} \tag{8}$$

The power oscillations in the frequency domain have multiple peaks due to the ramp and step motion profiles, here only the main peak has been considered. The reactor power is measured through eight He-3 proportional counters positioned in the channel 3-4 and 5-6. Power spectral densities of the power oscillations, $P_{\mathrm{A}}(\omega)$, $P_{\mathrm{B}}(\omega)$, are computed as the area below the peak in the frequency domain (see Fig. 9). The uncertainty associated to the power peaks comes only from averaging the results of the eight sensors, as the contribution due to the sensors dead time as not been considered. The power drift of the reactor due to temperature was corrected. Despite the large number of particles used to simulate this experiment, the uncertainties on the inserted reactivity (see again Fig. 8), resulted in significant errors for the reactivity time series, $\rho(\omega)$, of these samples. Despite that, the data shown in Fig. 8 were fitted in order to obtain the reactivity time series in the frequency domain.

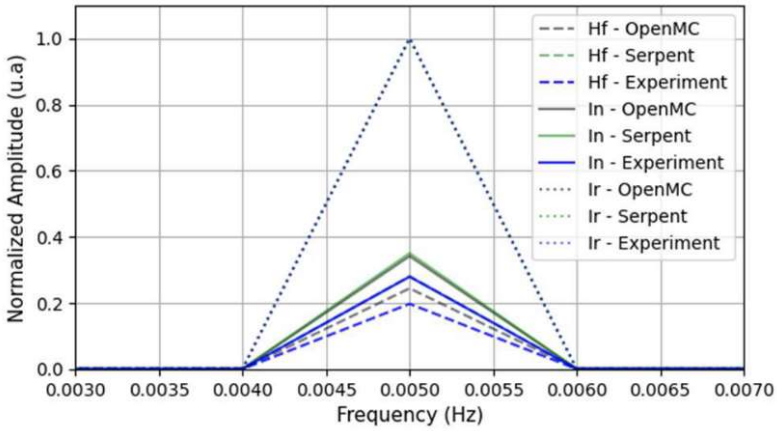


Figure 9: Power and reactivity transform for a step with f = 0.005 Hz.

Table 2 shows the percentage deviations respect to unity, see Eq. 9, of the ratios between the reactivity-ratio matrix elements, $\rho_{\mathrm{AB}}$, as obtained by OpenMC and Serpent and the corresponding elements of the power-ratio matrix, $\mathrm{P}_{AB}$, (experimentally obtained) for the case of the frequency $f_1 = 0.005$ Hz.

$$\left|\frac{(\rho_{AB})_{\,\mathrm{OpenMC}}}{(\mathrm{P}_{AB})_{\,\mathrm{exp}}} - 1\right| * 100\% \; ; \; \left|\frac{(\rho_{AB})_{\,\mathrm{Serpent}}}{(\mathrm{P}_{AB})_{\,\mathrm{exp}}} - 1\right| * 100\% \tag{9}$$

Since the results for the frequency $f_2 = 0.047$ Hz are very similar, we skip to report them. Results for the constant speed motion profile show a larger deviation (40-60%), especially, for the case of indium. The indium power spectral density amplitude of the power oscillations, $P(\omega)$, is similar to that of iridium and around four times larger than that of hafnium. However, this is not compatible with that given by the simulations where the reactivity time series of indium and hafnium produce similar results.

The investigation of deviations for the speed constant profile is undergoing as effects of scattering must be analysed as the sample spends a large timespan in the region where the gradient is maximum. Therefore, the combined effects of scattering and absorption is present. Despite, repeatability of the measurement was done for the indium sample with constant speed motion, it did not provide the same results as hafnium despite its similar absorption worth.

| A \ B | | Hf | In | Ir |
|---|---|---|---|---|
| Hf | OpenMC | 0.0 | 10.4 | 9.3 |
| | Serpent | 0.0 | 23.8 | 18.5 |
| Ir | OpenMC | 9.4 | 0.0 | 3.3 |
| | Serpent | 19.2 | 0.0 | 16.4 |
| Ir | OpenMC | 10.3 | 22.7 | 0.0 |
| | Serpent | 3.5 | 19.7 | 0.0 |

Table 2: Percentage error for a step profile with f = 0.005 Hz

A different approach is needed to accomplish the third and, partially, the second objectives. The small reactivity inserted by thin samples of copper, gold, graphite, and zirconium (less than 1 ct) produces a reactivity time series (see Eq. 7) impractical for our experiment. To overcome this problem, specific OpenMC and Serpent fixed-source simulations have been done for materials with low signal-to-noise ratio. Consider a sphere with a radius $R$ much larger than the thickness, $t$, and the radius, $r$, of the samples which are positioned at its centre.
The samples are then irradiated by neutrons emitted isotropically within the sphere volume, with an energy spectrum equal to that obtained by Serpent and OpenMC in the positions taken by the samples in the reactor. With such an approach, it is possible to calculate the reaction rates of the samples with a much larger accuracy and compare their ratio with that obtained experimentally with the power oscillation method (see Eq. 6).

In the case of the step motion profile, the above simulations are performed with the neutron energy spectrum at the centre, $X_{0\mathrm{cm}}(E)$, and at the outer position, $X_{20\mathrm{cm}}(E)$ when running the simulation. Then, the total absorption reaction rate is the weighted average of the reaction rates obtained with these two neutron spectra, where the weight is $\varphi^2(x)$ at the two positions in the reactor (see. Eq. 10).

$$\Sigma_{\mathrm{a}} = \frac{\left(\Sigma_{\mathrm{a}}(0)\varphi^2(0) + \Sigma_{\mathrm{a}}(20)\varphi^2(20)\right)}{\varphi^2(0) + \varphi^2(20)} \tag{10}$$

By this way, it is possible to validate the spectrum obtained in the centre and outer region of the AKR-2 reactor by means of the simplified MC models. For the linear ramp model, the neutron spectrum calculated by Serpent and OpenMC at every 2 cm starting from $x = 0$ up to $x = 20$ is used to run the sphere simulations. The terms $\Sigma_{\mathrm{a}}(2)\varphi^2(2), \Sigma_{\mathrm{a}}(4)\varphi^2(4), \ldots$ are computed. As it was defined the reactivity matrix, $\boldsymbol{\rho}_{\mathbf{AB}}(\omega)$ , similarly it can be defined the cross section matrix $\boldsymbol{\Sigma}_{\mathbf{AB}}$, whose elements are obtained according to the right-hand side of Eq. 6, and compare it with the experimental power matrix $\mathbf{P}_{\boldsymbol{AB}}(\omega)$, as shown by Eq. 11.

$$\left|\frac{(\Sigma_{AB})_{\ \mathrm{OpenMC}}}{(\mathrm{P}_{AB})_{\ \mathrm{exp}}} - 1\right| * 100\% \,;\ \left|\frac{(\Sigma_{AB})_{\ \mathrm{Serpent}}}{(\mathrm{P}_{AB})_{\ \mathrm{exp}}} - 1\right| * 100\% \tag{11}$$

| A\B | Ir | In | Au | Hf | Cu | Zr | C |
|---|---|---|---|---|---|---|---|
| Ir | 0.0 | 9.9 | 10.4 | 25.7 | 37.5 | 22.3 | 105 |
| In | 11.0 | 0.0 | 0.5 | 39.5 | 30.6 | 35.8 | 106 |
| Au | 11.6 | 0.5 | 0.0 | 30.2 | 30.3 | 36.5 | 106 |
| Hf | 20.4 | 28.3 | 28.7 | 0.0 | 50.3 | 2.7 | 104 |
| Cu | 60.0 | 44.1 | 43.4 | 101 | 0.0 | 95.7 | 109 |
| Zr | 18.3 | 26.4 | 26.7 | 2.7 | 48.9 | 0.0 | 104 |
| C | 1808 | 1639 | 1631 | 2247 | 1168 | 2190 | 0.0 |

Table 3: Percentage error for OpenMC spectrum

Tables 3 and 4 present the comparison according to Eq. 11 for the step motion profile with the frequency of 0.005 Hz. This frequency was preferred as it was able to amplify the signals coming from thin samples of gold and copper. Large errors appear for zirconium and graphite due to their low signal-to-noise ratio. Despite that, this method allows measuring integral cross sections of small samples for absorbing materials, like indium and iridium, as well as to obtain reasonable estimates for non-strong absorbers (e.g. Au, Cu).

| **A\B** | Ir | In | Au | Hf | Cu | Zr | C |
|---|---|---|---|---|---|---|---|
| Ir | 0.0 | 4.2 | 8.9 | 19.6 | 36.6 | 15.7 | 105 |
| In | 4.4 | 0.0 | 4.9 | 24.8 | 33.8 | 20.8 | 109 |
| Au | 9.8 | 5.2 | 0.0 | 31.2 | 30.4 | 27.0 | 109 |
| Hf | 16.4 | 19.9 | 23.8 | 0.0 | 47.0 | 3.2 | 107 |
| Cu | 57.7 | 51.1 | 43.6 | 88.5 | 0.0 | 82.4 | 113 |
| Zr | 13.6 | 17.2 | 21.3 | 2.7 | 45.2 | 0.0 | 107 |
| C | 1256 | 1208 | 1150 | 1482 | 833 | 1438 | 0.0 |

Table 4: Percentage error for Serpent spectrum

## 5. Conclusions

The simplified model of the reactor provides acceptable results for most of the experiments performed at AKR-2, allowing the reactor's users to compare their experimental practices with Serpent and/or OpenMC simulations. It provides accurate results in the critical experiment (although some assumptions were necessary), rod worth curves, and radial flux distribution in the core and part of the reflector region. Finally, it also demonstrated a useful tool for the pile oscillator experiment. Good results were achieved for the step motion profile. Nevertheless, the large errors found for the ramp motion profile require further investigation. The influence of phenomena like scattering, slowing down and diffusion are, at present, not considered. The pile oscillator method is a valuable tool for integral cross section measurements, further investigations will explore the possibility of using this method to obtain tabulated data, e.g., thermal microscopic cross sections or resonance integrals.

## 6. Acknowledgment

This work is part of the research project NAUTILUS funded by the German Federal Ministry of Education and Research (BMBF) under the reference number 02NUK079.

## 7. References

[1] Technical University Dresden. (2019). "Experiments in Reactor Physics and Radiation Protection. Faculty of Mechanical Science and Engineering". Institute of Power Engineering. Dresden, Germany. Retrieved from http://tu-dresden.de/mw/akr.

[2] Lange, C., Bernt, N. (2018). "The education and research reactor AKR-2 and its experimental programme for education" in PHYSOR 2018: Reactor Physics paving the way towards more efficient systems, Cancun, Mexico, April 22-26, 2018.

[3] M. Viebach, A. Knospe, C. Lange, B. Merk, A. Hurtado. NAUTILUS: A project for the Development of Experimental Methods for Investigating Innovative approaches to Nuclear Waste Management and to Nuclear Safety. PHYSOR 2024 – Beyond the Blue Print: Pioneering Reactor Physics for Real-World Implementation, San Francisco, CA, USA.

[4] Leppänen, J., et al. (2015) "The Serpent Monte Carlo code: Status, development and applications in 2013". Ann. Nucl. Energy, 82 (2015) 142-150.

[5] Paul K. Romano, Nicholas E. Horelik, Bryan R. Herman, Adam G. Nelson, Benoit Forget, and Kord Smith, "OpenMC: A State-of-the-Art Monte Carlo Code for Research and Development," Ann. Nucl. Energy, 82, 90–97 (2015).

[6] Brown, D.A. et al. (2018). ENDF/B-VIII: 0: the 8th major release of the nuclear reaction data library with CIELO-project cross sections, new standards. Nuclear Data Sheets, 148, 1-142.

[7] Hoover, J. I. et al. (1948). Measurement of neutron absorption cross sections with a pile oscillator. Physical Review, 74(8), 86.